Egyptian Journal of Radiology and Nuclear Medicine

RESEARCH

Open Access

Predictors of breast cancer HER2-receptor positivity by MRI intuitive imaging features

Dalia Bayoumi[1], Ahmed Alaa EL-Din ELagamy[1], Hesham Sabry Mohamed Salem[1] and Aya Elboghdady[1*]

Abstract

Background Today, breast cancer is the most diagnosed cancer worldwide. There are many different clinical presentations, radiological characteristics, and histological types of breast cancer. HER2 is overexpressed in a significant number of breast cancer cases reaching 20% of all breast cancers, and its overexpression is seen directly proportionate with a poor outcome and prognosis.

Methods We started this cross-sectional research from January 2022–December 2023 on 202 breast cancer patients who had 220 lesions. The molecular subtypes of the different lesions were determined in all the included cases. Magnetic resonance imaging (MRI) studies were conducted in all included cases. The MRI parameters included conventional MRI, diffusion-weighted analysis, and dynamic post-contrast T1-weighted imaging.

Results The prevalence of irregular margins ($P<0.001$), linear and segmental distribution ($P=0.044$), heterogeneous pattern ($P<0.001$), and type 2 curve was statistically significantly higher in the HER2-positive lesions. Nipple infiltration incidence showed statistically significant elevation in the HER2-positive lesions ($P=0.017$). The lesions' ADC and perilesional ADC in the HER2-positive lesions were also statistically significantly elevated. The best cutoff point of ADC to detect lesions with positive HER2 expression was > 0.885 × 10–3 mm_2/s, with 65.7% sensitivity and 60% specificity, with a statistically significant value ($p=0.005$).

Conclusions Magnetic resonance imaging of breast imaging is a promising noninvasive method for identifying breast tumors with the HER2 molecular subtype. Combining various radiological features by MRI may provide a conclusion for recognizing positive HER2 lesions.

Keywords Breast cancer, Molecular subtypes, HER2, ADC

Background

Breast cancer is the most common type of cancer among women worldwide [1]. In developing countries, particularly in the Middle East, it is considered the leading cause of cancer death in women [2].

Immunohistochemical subtypes are widely used to classify breast cancers which in turn depend on receptors' expression such as estrogen receptor (ER), progesterone receptor (PR), and/or human epidermal growth factor receptor 2 (HER2/neu or ErbB2). This helps in determining their prognosis and therapy as well [3].

Hormone receptor (HR) positivity, which is the combined result of both ER and PR positivity, is the most prevalent molecular subtype of invasive breast cancer. The greatest survival rates are seen in HR-positive tumors [4].

Before the emergence of HER2-receptor-targeted therapeutic agents, cases displaying positive HER2 breast cancer had an overall poor outcome [5]. Preoperative targeted agents use can downstage the surgical decision from total mastectomy to just lumpectomy and also reduce the axillary surgery extent, from axillary lymph node dissection to the less invasive sentinel lymph node biopsy [6]. Moreover, the effectiveness of the neoadjuvant

*Correspondence:
Aya Elboghdady
ayabogdady@mans.edu.eg
[1] Department of Radiology, Faculty of Medicine, Mansoura University, Mansoura, Egypt

therapy may determine whether further adjuvant therapy is needed [7].

In the context of neoadjuvant chemotherapy (NACT) for early-stage HER2-positive tumors, the radiologist assesses imaging characteristics that are related to the disease trajectory and surgical treatment. Mammography, ultrasound (US), and magnetic resonance imaging (MRI) are important imaging modalities for evaluating HER2-positive malignancies and their response to therapy [8].

MRI has surfaced as an important imaging modality in HER2-positive breast cancer assessment. Recent studies have discussed its potential to determine the molecular subtype of breast cancer, in particular HER2 overexpression. This information can be helpful for surgeons and clinicians to make informed decisions before starting treatment and can reduce the time and cost of possible further tests, especially in cases where results are equivocal and more expensive tests are required at central laboratory facilities [9].

Aim of work

To evaluate whether breast MRI could determine the HER2 molecular subtype of breast cancers and to identify biomarkers for intuitive imaging features, this will have a great impact on patients' management and prognosis.

Methods

The Institutional Research Board approved our research work.

Study design

This study was conducted between March 2022 and December 2023. The inclusion criteria were female patients with various molecular subtypes of pathologically confirmed breast cancer with accurate clinical data for each case. The exclusion criteria were patients who have undergone neoadjuvant chemotherapy, patients who had a recent breast biopsy (within one month), patients who had absolute contraindications for undertaking an MRI scan (like patients who had metallic prosthesis or cardiac pacemaker), patients who had renal function impairment, and patients who experience claustrophobia.

The research was performed following Helsinki Standards as declared in 2013 [10].

Study tools

- After a local examination of the breast and the axilla, a complete history was acquired from all the cases. Apart from the standard investigations, we also focused on the histopathological diagnosis and its molecular subtypes, such as tumor histopathological type, Bloom–Richardson tumor grade, the presence or absence of lympho-vascular emboli, estrogen receptor (ER), and progesterone receptor (PR), HER2-neu receptor and Ki67 assessment.

MRI procedure

- All MRI studies were conducted using (MRI Phillips 1.5 T). Following international recommendations, MRI was performed for all these women as a part of our institution's standard preoperative work-up.
- For pre-menopausal women, the examination was scheduled to take place between days 7 and 14 of the menstrual cycle. To reduce aliasing artifacts and phase encoding artifacts, we position the patient so that her arms are comfortably above her head. The use of foam wedges inside the coil to reduce respiratory movement artifacts was implemented when the breast volume was low.
- To achieve symmetrical reading, we examined both breasts simultaneously to improve our ability to detect physiological glandular contrast uptake; however, this technique reduces the diagnostic value of the exam because it masks a certain amount of contrast uptake and eliminates aliasing artifacts, which happens when our field of view is smaller than the area of the patient being explored. The pixel size on each side was less than 1 mm, and the slice thickness was 3 mm. A voxel that is less than 1 mm and isotropic is ideal for multiplanar reconstruction.
- To reduce respiratory and cardiac movement artifacts in axial plane acquisitions, phase encoding was done from right to left. Non-contrast imagining was used at the beginning of the scan. It incorporated taking axial weighted images in T1 and T2, with adipose tissue signal suppression by STIR followed by diffusion-weighted imaging (DWI), and lastly dynamic contrast-enhanced magnetic resonance imaging (DCE-MRI).
- To obtain diffusion-weighted images before dynamic images, single-shot spin-echo EPI sequences with TR/TE/NEX: 5800/139 ms and different b values of 0, 500, and 1000 mm^2/sec were used to acquire the standard T2-weighted images added with strong diffusion gradients. The *X*, *Y*, and *Z* directions are the three orthogonal directions in which the diffusion gradients were applied successively. All images had sections with a thickness of 4 mm, an inter-slice gap of 1 mm, a field of view of 300–360 mm, and a 128×256 matrix. The acquisition took 120 s in total.

In every instance, orthogonal (DWI) images and ADC maps were acquired.

- For every section, four sets of DWI were acquired. The sensitization gradients were applied successively in the *X*, *Y*, and *Z* planes, as shown by the first three sets of images (trace images). The final set (ADC map), which corresponds to the average diffusion images, allows one to measure the ADC at any point or ROI. After obtaining the trace images at various *b* values (*b* value (0), *b* value (500), and *b* value (1000), the MRI scanner software computed the ADC maps.
- Every dynamic study was conducted in the axial plane using fat-saturated pulse therapy to suppress fat. The FLASH 3 D GRE-T1W1 sequence was utilized, and its parameters were as follows: flip angle of 20–25°, slice thickness of 3 mm without any inter-slice gap, a field of view (FOV) of 300–360 mm, and matrix size of 384 × 384.
- An automated injector injected gadopentetate dimeglumine (gadolinium) into the antecubital vein via an intravenous cannula with a gauge of 18–20 ml per second after the pre-contrast study. The dose of gadolinium was between 0.1 and 0.2 mmol/kg. The next step was to inject 20 ml of saline at a rate of 3–5 ml/sec.
- Every dynamic scan had a pre- and post-contrast series, every one lasting approximately for 1.2 min. The initial two acquisitions, denoted as wash-in rate, marked the early contrast uptake, whereas the subsequent acquisitions, denoted as washout kinetics, showed delayed enhancement.
- Images post-processing: making time-to-signal intensity curves (TIC) for lesions that show enhancement and in-line images subtraction using the MIP algorithm in different projections (axial, coronal, and sagittal).

Imaging analysis

Image analysis was conducted by at least two experienced radiologists (7–12 years of experience). Images were interpreted regarding lesions' morphology, as a mass, non-mass enhancement, or focus. Lesions numbers were evaluated as either single or multiple. Then, the imaging characteristics of each lesion were evaluated mass lesions and were described in terms of (I) *shape* (rounded, oval, or irregular masses), (II) *margins* (circumscribed, irregular, or speculated), (III) *internal enhancement characteristics* (*homogeneous, heterogeneous, marginal, dark "non-enhancing" internal septations).* While non-mass lesions were described in terms of (I) *distribution* (focal, linear, ductal, segmental, regional, and diffuse enhancement) and (II) *internal enhancement pattern* (homogenous, heterogeneous, clumped, clustered ring enhancement). Also, all the lesions were assessed to detect if they showed nipple or chest wall infiltration. Background parenchymal enhancement was classified into (minimal, mild, moderate, and marked). Enhancement dynamics (kinetics) analysis: by evaluating time signal intensity curve data. Accordingly, we identified three curve types: type 1 (persistent dynamic curve—more than 10% with time), type 2 (plateau dynamic curve—does not alter following initial rise), or type 3 (washout dynamic curve—reduces more than 10%). Then, lesions were detected on DWI & ADC maps after evaluating the source images and using them for guidance. Afterward, lesions were delineated according to their signal intensity on b1000 images and classified into free diffusion (displaying low signal intensity) or restricted diffusion (displaying high signal intensity). Automatic measurements of ADC values followed (minimum 3 ROIs), calculating the mean ADC afterward and expressing it as 10^{-3} mm^2/sec.

Statistical analysis

Study data were analyzed using Statistical Package for Social Sciences (SPSS) version 25 for Windows (IBM, SPSS Inc, Chicago, IL, USA). Categorical data were expressed in number and percent. The Chi-square test (Monte Carlo test or Fischer's exact test) made the comparison between two or more groups with categorical data. The quantitative data were tested whether normally distributed or not by using the Kolmogorov–Smirnov test and were expressed as median ± SD if was parametric or median (range) if nonparametric.

The independent samples *t*-test was used to compare two groups with quantitative variables that were regularly distributed, and the Mann–Whitney *U*-test was employed if the data were abnormally distributed. The receiver operator characteristic (ROC) curve was used to detect the best cutoff point of the quantitative variable in differentiating two classes of binary categorical outcomes. *P* values < 0.05 are considered significant.

Results

The study enrolled 202 females with breast cancer recruited from the Oncology center. Cases ages ranged from 27 to 74 years with mean age of the cases of 46.32 ± 11.29 years. The age group most represented was between 41 and 50 years old (34.7%), with 24.8% of respondents falling into this category.

The current study's molecular type analysis revealed that triple negative (TN) was present in 28 lesions (12.7%), luminal A was present in 58 lesions (26.4%), luminal B was present in 64 lesions (29.1%) (Fig. 1), HER2 positive was found in 70 lesions (31.8%) (Figs. 2 and 3).

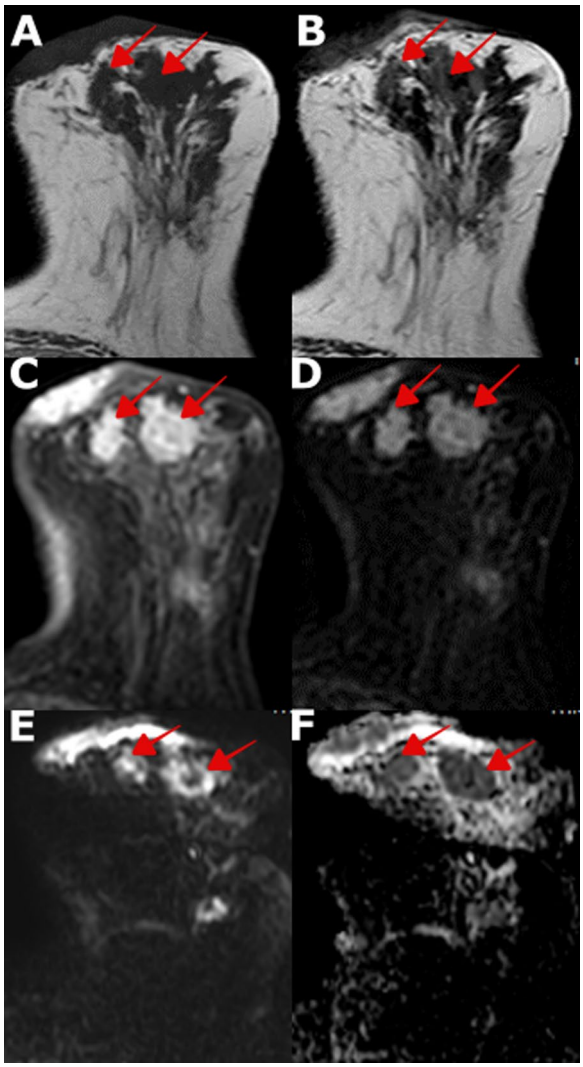

Fig. 1 Female patient aged 67 years old complaining of a left breast lump. She had a family history of breast cancer (mother), and she had not received hormonal contraception before. MRI revealed: **A** & **B** Pre-contrast T1- and T2-weighted axial image showing: Multicentric masses with irregular shape and margin associated with thickened overlying skin at the left breast's upper outer quadrant (UOQ). **C** & **D** Post-contrast dynamic and subtraction axial images showing: heterogeneously enhancing masses with thickened enhanced overlying skin as well as clumped segmental non-mass enhancement at the UOQ of the left breast. **D** & **E** DWI of the lesion shows high signal intensity and low signal in ADC map with mean lesion ADC value measured at largest lesion = 0.79×10^{-3} mm/sec and perilesional ADC = 1.4×10^{-3} mm/s. Pathology proved to be Grade II invasive duct carcinoma—Luminal A subtype—Ki-60%

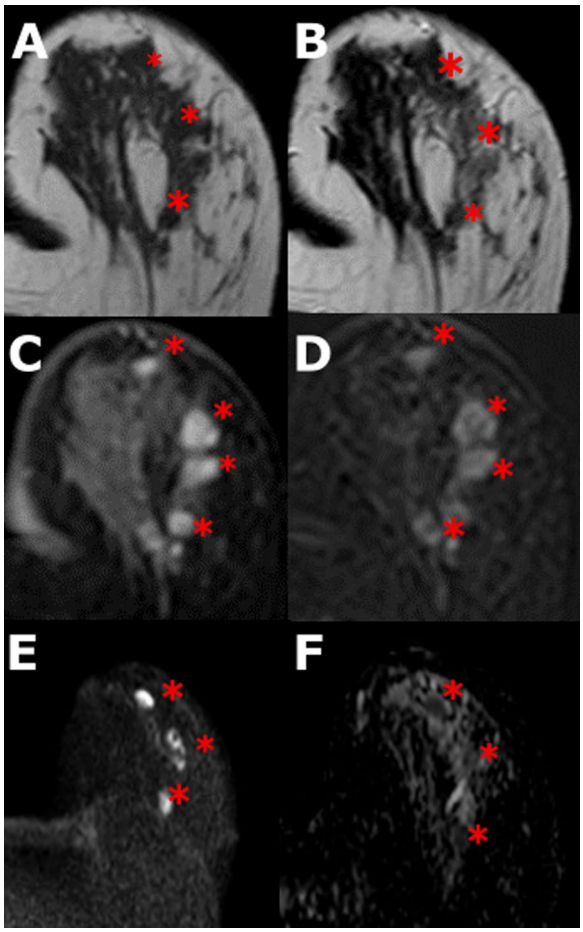

Fig. 2 Female patient aged 35 years old complaining of left breast mass with no known family history of breast cancer. MRI revealed: **A** & **B** Pre-contrast T1- and T2-weighted axial images showing: multifocal mass of irregular shape and margin seen at the lower half of left breast displaying low signal intensity on T1 and intermediate to low SI on T2-weighted images. **C** & **D** Post-contrast dynamic and subtraction axial images showing: heterogeneous enhancing multifocal mass seen at the lower half of the left breast. **E** & **F** DWI shows high signal and low signal in the ADC map, with mean lesion ADC value = 0.9 $\times 10^{-3}$ mm/sec and perilesional ADC = 1×10^{-3} mm/s. Pathology proved to be high-grade invasive duct carcinoma—Luminal B HER2-positive subtype—Ki-30%

Additionally, HER2 (Fig. 4) was positive in 134 lesions (60.9%), PR was positive in 114 lesions (51.8%), and ER was positive in 122 cases (55.5%). The range of the KI percent was 5–90%, with a mean of 37.21 ± 20.85%. Detailed clinical and histopathological data are shown in Table 1.

After comparing HER2-positive lesions and other molecular subtypes lesions, there was no statistically significant difference between the cases with HER2-positive lesions and other types; regarding the shape of the mass lesions ($p = 0.200$), the pattern of mass enhancement ($p = 0.160$), the incidence of chest wall infiltration ($p = 0.332$), and background parenchymal enhancement (BPE) ($p = 0.169$).

On the other hand, the prevalence of irregular margins was statistically significantly higher in the HER2-positive lesions ($P < 0.001$). Also, the prevalence of linear

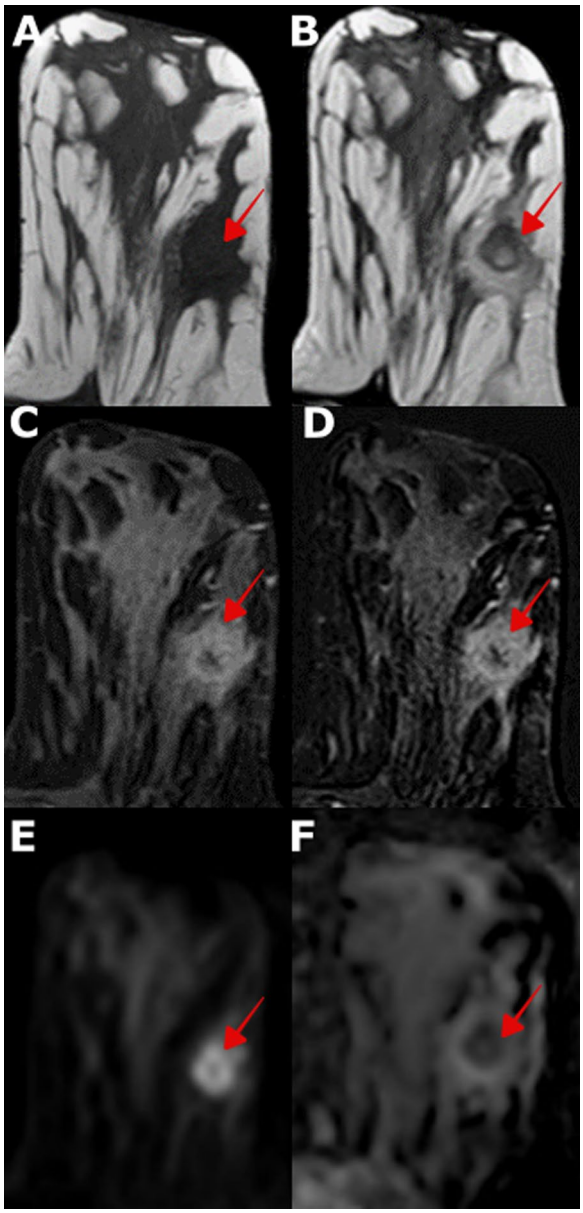

Fig. 3 A female patient aged 30 years old complaining of left breast lump. She had no previous family history of breast cancer, nor had she received hormonal contraception before. MRI revealed: **A** & **B** Pre-contrast T1- and T1-weighted axial images showing: a mass lesion of low signal intensity at the left breast's upper outer quadrant (UOQ) surrounded by peritumoral high signal intensity on T2 WI. **C** & **D** Post-contrast dynamic and subtraction axial images showing: marginal heterogeneous enhancement. at UOQ of the left breast. **E** & **F** DWI shows marginal high signal intensity with low signal in ADC map with mean lesion ADC value = 0.85×10^{-3} mm/sec and perilesional ADC = 1×10^{-3} mm/sec. Pathology proved to be high-grade invasive ductal carcinoma—Triple-negative subtype—Ki-60%

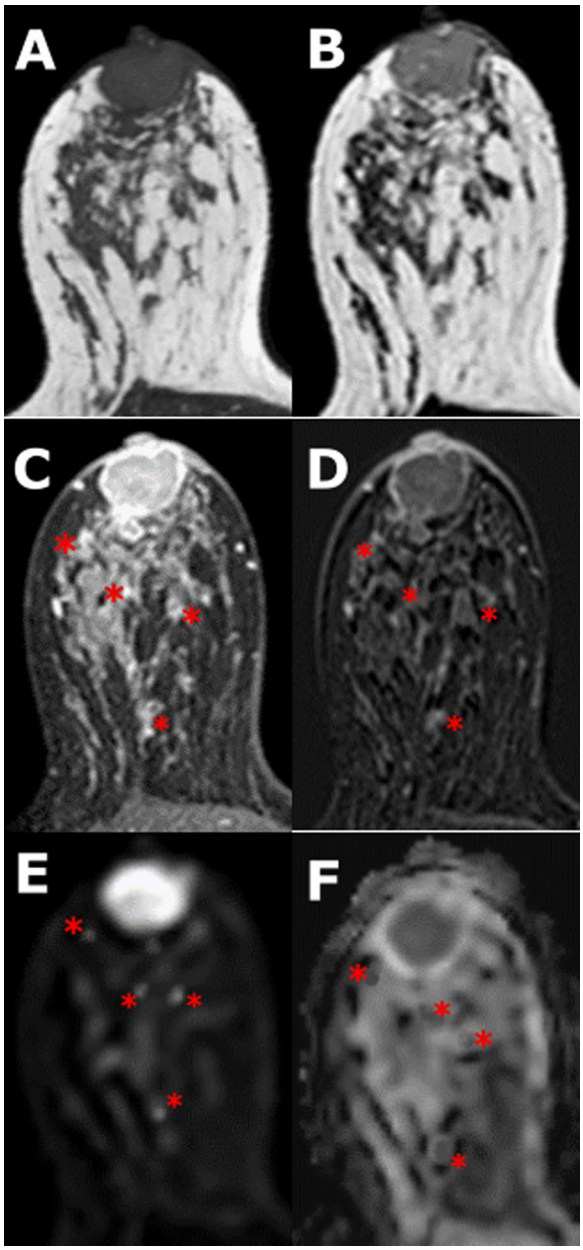

Fig. 4 Female patient aged 50 years old complaining of a right painful breast lump with a family history of breast cancer (sister). MRI revealed: **A** & **B** Pre-contrast T1- and T2-weighted axial image showing: a large retro-areolar breast mass with partially circumscribed margins infiltrating nipple-areolar complex and smaller satellite lesions, displaying low signal intensity on T1 and intermediate to low signal intensity on T2-weighted images. **C** & **D** Post-contrast dynamic and subtraction axial images showing: heterogeneous enhancement of retro-areolar mass infiltrating the nipple-areolar complex with enhancing satellite lesions. **E** & **F** DWI shows high signal intensity with low signal in ADC map with mean lesion ADC value = 0.7×10^{-3} mm/sec and perilesional ADC = 1.5×10^{-3} mm/sec. Pathology proved to be Grade II invasive duct carcinoma—HER2 subtype—Ki-30%

Table 1 Clinical and histopathological data of the study cases

Variables	Number of cases $N=202$	
Age (years) (Number of cases = 202)		
Mean ± SD	46.32 ± 11.29	
Median (Range)	44 (27–74)	
Age groups		
≤ 30 years	14	6.9
31–40 years	50	24.8
41–50 years	70	34.7
51–60 years	46	22.8
61–70 years	16	7.9
> 70 years	6	3
Molecular types		
HER2	70	31.8
LUMINAL B	64	29.1
LUMINAL A	58	26.4
TN	28	12.7
ER		
Negative	98	44.5
Positive	122	55.5
PR		
Negative	106	48.2
Positive	114	51.8
HER2		
Negative	86	39.1
Positive	134	60.9
KI (%)		
Mean ± SD	37.21 ± 20.85	
Median (Range)	30 (5–90)	

HER2 human epidermal growth factor 2, *TN* triple negative, *ER* estrogen receptor, *PR* progesterone receptor

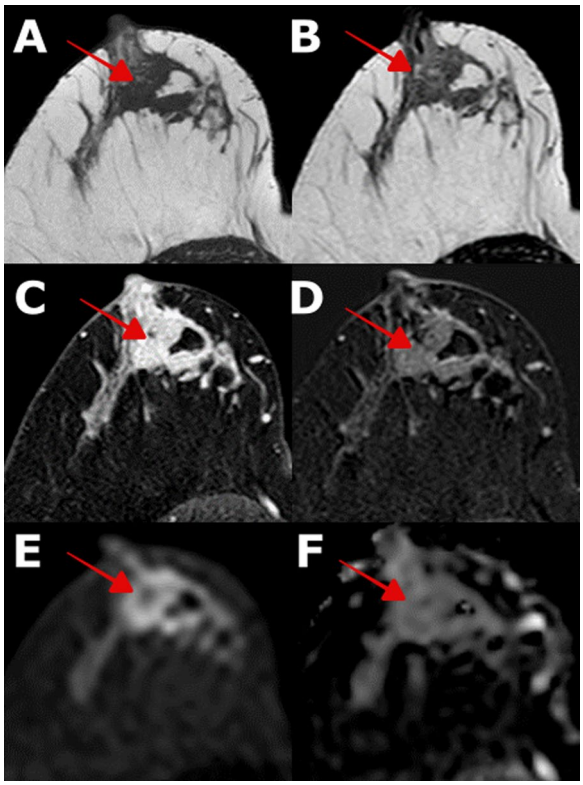

Fig. 5 Female patient aged 28 years old complaining of right breast lump with no family history of breast cancer. MRI revealed: **A** & **B** Pre-contrast T1- and T2-weighted axial image showing: large mass with irregular margin seen at the inner half of the right breast infiltrating the nipple-areolar complex. **C** & **D** Post-contrast dynamic and subtraction axial images showing: a large heterogeneous enhancing mass seen at the inner half of the right breast infiltrating the nipple-areolar complex with related medially located segmental non-mass enhancement. **E** & **F** DWI shows high signal intensity with low signal in ADC map with mean lesion ADC value = 0.9×10^{-3} mm/sec and perilesional ADC = 1.18×10^{-3} mm/sec. Pathology proved to be Grade III invasive duct carcinoma associated with extensive high-grade ductal carcinoma in situ—HER2 subtype—Ki-30%

and segmental distributions was statistically significantly higher in the HER2-positive lesions ($P=0.044$).

The most common enhancement pattern detected in HER2-positive lesions was a heterogeneous enhancement pattern. The incidence of nipple infiltration was statistically significantly higher in the HER2-positive lesions (Fig. 5) ($P=0.017$).

Type 2 curve was more prevalent in the HER2-positive lesions with a statistically significant difference ($P<0.001$). Finally, the lesion ADC and perilesional ADC were statistically significantly higher in the HER2-positive lesions. Table 2 shows a more descriptive analysis of HER2-positive lesions versus other molecular lesion types.

We also assessed the diagnostic value of HER2-positive lesion ADC as well as perilesional ADC. Regarding lesion ADC, by ROC curve the best cutoff point of ADC to identify lesions with positive HER2 expression was > 0.885×10^{-3} mm_2/s, with 65.7% sensitivity and 60% specificity, with a statistically significant value ($p=0.005$), while perilesional ADC; the best cut-off point of perilesional ADC to identify lesions with positive HER2 expression was > 1.25×10^{-3} mm_2/s, with 48.6% sensitivity and 55.7% specificity, with non-statistically significant value ($p=0.056$). This is described in Table 3 and Fig. 6.

With univariate regression analysis, irregular margins, linear distribution, absence of regional pattern, segmental distribution, heterogeneous pattern, nipple infiltration, multiple number of lesions, decreased representation of type 3 curves, increased ADC value, and increased perilesional ADC values were considered as diagnostic features of HER2 molecular types. However,

Table 2 Comparison of the molecular types of all breast lesions

	HER2 [*N* = 70]	Other types [*N* = 150]	Test of significance
Mass (*n* = 134)	*N* = 26	*N* = 108	
Shape			
Oval	4 (15.4%)	6 (5.6%)	MC = 3.220 *P* = 0.200
Rounded	2 (7.7%)	6 (5.6%)	
Irregular	20 (76.9%)	96 (88.9%)	
Margin (n = 134)			
Speculated	22 (84.6%)	100 (92.6%)	MC = 18.688 *P* < 0.001*
Irregular	4 (15.4%)	0 (0%)	
Circumscribed	0 (0%)	8 (7.4%)	
Enhancement pattern			
Heterogeneous	26 (100%)	102 (94.4%)	FET = 1.324 P = 0.160
Marginal	0 (0%)	6 (5.6%)	
Non-mass (*n* = 86)	*N* = 44	*N* = 42	
Distribution			
Diffuse	0 (0%)	2 (4.8%)	MC = 5.874 *P* = 0.044*
Linear	6 (13.6%)	0 (0%)	
Regional	0 (0%)	14 (33.3%)	
Segmental	38 (86.4%)	26 (61.9%)	
Enhancement pattern			
Heterogeneous	44 (76.9%)	42 (38.9%)	$\chi 2 = 16.279$ P < 0.001*
Chest wall infiltration	0 (0%)	2 (1.3%)	FET = 0.942 P = 0.332
Nipple infiltration	16 (22.9%)	16 (10.7%)	$\chi 2 = 5.706$ P = 0.017*
Number of lesions			
Single	54 (77.1%)	90 (60%)	$\chi 2 = 6.202$ *P* = 0.013*
Multiple	16 (22.9%)	60 (40%)	
BPE			
Minimal	2 (2.9%)	2 (1.3%)	MC = 5.035 *P* = 0.169
Mild	40 (57.1%)	92 (61.3%)	
Moderate	26 (37.1%)	56 (37.3%)	
Marked	2 (2.9%)	0 (0%)	
Curve			
Type 2	42 (60%)	50 (33.3%)	$\chi 2 = 13.949$ *P* < 0.001*
Type 3	28 (40%)	100 (66.7%)	
Lesion ADC [$\times 10^{-3}$ mm_2/s]	0.937 ± 0.165	0.875 ± 0.143	*t* = 2.847 *P* = 0.005 *
Perilesional ADC [$\times 10^{-3}$ mm_2/s]	1.307 ± 0.248	1.229 ± 0.204	*t* = 2.442 P = 0.015*

BPE background parenchymal enhancement, *ADC* apparent diffusion coefficient, *t* Independent samples *t*-test, *MC* Monte Carlo test, $\chi 2$ Chi-square test, *FET* Fischer's exact test

* Statistically significant ($p < 0.05$)

with multivariate regression analysis, the absence of regional pattern, heterogeneous pattern, and decreased representation of type 3 curves was shown as independent diagnostic features of HER2 molecular types, as shown in Table 4.

Discussion

The goal of the current study was to identify intuitive imaging features as potential biomarkers and assess whether breast magnetic resonance imaging could reflect the HER2 molecular subtype of breast cancers.

Table 3 Diagnostic value of lesion and perilesional ADC [$\times 10^{-3}$ mm^2/s] to identify cases with positive HER2

Diagnostic criteria	Lesion ADC [$\times 10^{-3}$ mm_2/s]	Perilesional ADC [$\times 10^{-3}$ mm_2/s]
AUC	0.619	0.580
Cutoff point	> 0.885	> 1.25
Sensitivity	65.7%	48.6%
Specificity	60%	55.4%
NPV	66.3%	52.4%
PPV	62.4%	51.6%
Accuracy	64.2%	50.4%
P	0.005*	0.056

AUC area under the curve, *NPV* Negative predictive value, *PPV* Positive predictive value, *P* probability

* significant *p*-value (< 0.005)

The study included 202 pathologically proven cancer breast patients with different molecular subtypes. Cases' age varied from 27 to 74 years with a mean age of 46.32 ± 11.29 years. Between the ages of 41 and 50 (34.7%) were the age group with the highest representation, followed by 31–40 (24.8%).

This was consistent with an age distribution for cases reported in another study by Metwally et al., where the mean age was 41.3 years [11]. This was also in line with the findings of Ng et al., who discovered that the age group of 20–40 years was the next largest, with most patients falling into the 41–60 age range [12].

Previous reports stated that 1–40% of HER2 BC have pathological intratumor heterogeneity related to variations in HER2 expression levels [13, 14]

In the current study, the molecular type was found to be HER2 positive in 70 cases (31.8%), 64 cases (29.1%) for luminal B, 58 cases (26.4%) for luminal A, and 28 cases (12.7%) for TN tumors. This was consistent with a different study by Darwish et al. who found that 30.1% of cases had HER2-neu positivity [15].

The prevalence of HER2-positive breast cancer in the current study was slightly higher as compared to Algazzar et al. who included 60 cases their age ranged from 41 to 72 years and had a mean age of 56.48 ± 8.70. HR-positive receptors were found in 44 cases representing 73.3%, HER2/neu-positive receptors were found in 13 cases representing 21.7%, luminal A receptors were detected in 34 cases representing 56.7%, luminal B receptors were detected in 10 cases representing 16.7%, HER2/neu-enriched were detected in 7 cases representing 11.7%, and triple-negative breast cancer was found in 9 cases representing 15% [16].

HER2-positive overexpression at MRI scan often appears as a multifocal irregular mass with plateau or washout kinetics and non-mass enhancement, with a pooled odds ratio of 2.45. While oval masses with circumscribed margins, non-mass enhancement, and peritumoral edema characterize HR-negative HER2-positive cancers. Whereas HR-positive HER2-positive cancers have irregular shapes and spiculated margins [17, 18].

Many studies focused on the relationship between HER2 status and nipple involvement [19–22]. The HER2-positive group had a higher nipple involvement rate than the negative group (RR = 1.760, 95% CI = 1.463–2.116) as reported by Zhang et al. previous study [19]. This agrees with our results that showed nipple involvement in 22.9%

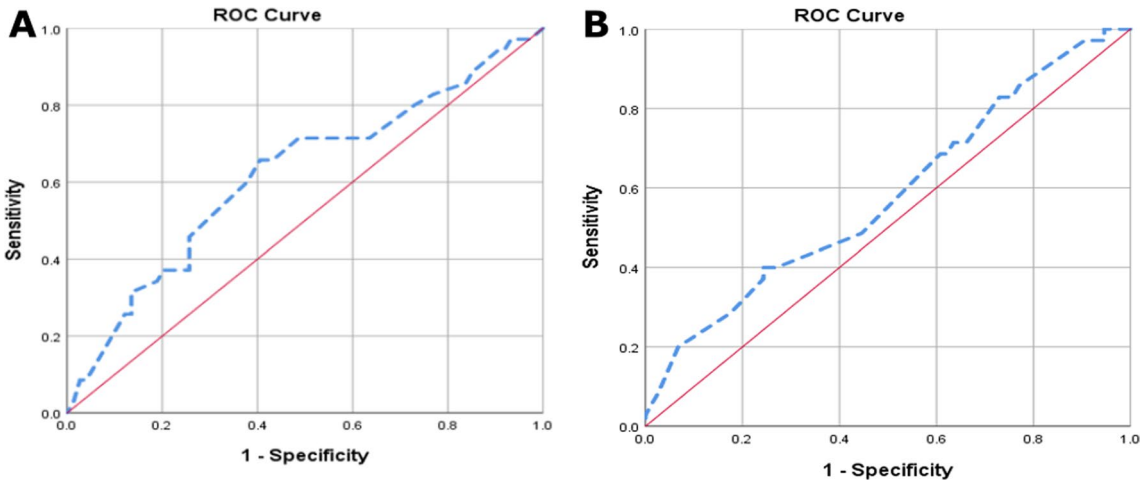

Fig. 6 Receiver operating curve (ROC) curve of ADC $\times 10^{-3}$ mm^2/s to identify cases with positive HER2. **A** lesion ADC and **B** perilesional ADC. Demonstrates that lesion ADC cutoff value of > 0.885 $\times 10^{-3}$ mm^2/s and AUC: 0.619 while perilesional ADC > 1.25 $\times 10^{-3}$ and AUC = 0.606. ADC: Apparent diffusion coefficient, AUC: area under curve

Table 4 Univariate and multivariate regression analysis for prediction of positive HER2

Predictors	Univariate regression				Multivariate regression			
	P value	Odds ratio	95% C.I. for odds ratio		*P* value	Odds ratio	95% C.I. for odds ratio	
			Lower	Upper			Lower	Upper
Oval	*R*							
Rounded	0.766	1.174	0.622	1.572				
Irregular	0.225	0.609	0.274	1.357				
Speculated	*R*							
Irregular	0.014*	1.472	1.355	1.755	0.214	1.23	0.71	1.46
Circumscribed	0.488	1.200	0.794	2.260				
Heterogeneous	*R*							
Marginal	0.078	0.329	0.095	1.135				
Diffuse	*R*							
Linear	0.040*	4.510	1.074	8.929	0.532	1.254	0.630	1.245
Regional	< 0.001*	0.466	0.325	0.668	0.001*	0.546	0.238	0.762
Segmental	0.002*	1.472	1.355	1.755	0.214	1.23	0.71	1.46
Heterogeneous	< 0.001*	1.648	1.255	2.187	< 0.001*	1.740	1.425	2.207
Chest wall infiltration	0.225	0.609	0.274	1.357				
Nipple infiltration	0.031*	2.147	1.479	2.436	0.096	1.030	0.887	1.257
Single	R							
Multiple	0.019*	0.403	0.188	0.863	0.289	0.712	0.380	1.334
Minimal	*R*							
Mild	0.882	0.716	0.128	1.487				
Moderate	0.331	0.320	0.032	3.184				
Marked	0.603	0.762	0.273	2.125				
Type 2	*R*							
Type 3	0.001*	0.092	0.022	0.379	0.005*	0.483	0.230	0.846
ADC	0.006*	4.266	1.129	5.348	0.532	1.254	0.630	1.245
Perilesional ADC	0.017*	2.833	1.324	7.648	0.452	1.327	0.580	1.397

CI Confidence interval, *OR* Odd's ratio

of the HER2-positive cases versus 10.7% of other molecular subtypes.

In the current study, there was a statistically significant higher prevalence of non-mass lesions in the HER2-positive lesions (62.9% versus 28%) ($p < 0.001$) with the segmental non-mass enhancement pattern was the prevalent pattern among non-mass lesions in our work, representing 86.4% of the cases. This agreed with Algazzar et al. who showed that there was a statistically significantly higher prevalence of non-mass lesions in the HER2-positive lesions (38.5% versus 12.8%) ($p = 0.049$) [16].

According to the current findings, there was no significant statistical difference between the HER2 and other molecular subtypes concerning lesions' size. This supported Mohammed et al. findings that HER2 status did not affect tumor size ($p = 0.745$) [23].

In the current study, heterogeneous enhancement was reported in all HER2-positive cases with mass lesions as compared to 94.4% in cases with HER2-negative lesions, with no statistically significant difference ($p = 0.160$). This was in line with Algazzar et al. who showed that heterogeneous enhancement was reported in 84.6% of the HER2-positive cases and 61.7% in HER2-negative lesions, with no discernible variation between the two categories ($p = 0.29$) [16].

The current results showed that irregular margins were statistically significantly higher in the HER2-positive cases (15.4% versus 0%) ($p < 0.001$). This copes with Algazzar et al. who showed that all cases with HER2-positive type had irregular shapes and non-circumscribed margins [16].

In our study, HER2-positive breast cancer showed statistically significantly higher lesional ADC value ($0.937 \pm 0.165 \times 10^{-3}$ mm_2/s versus $0.875 \pm 0.143 \times 10^{-3}$ mm_2/s) and perilesional ADC value ($1.307 \pm 0.248 \times 10^{-3}$ mm_2/s versus $1.229 \pm 0.204 \times 10^{-3}$ mm_2/s) as compared to other molecular subtypes. This was following López–García

and Rupa et al. demonstrated that although lesions with HER2-neu-positive cases had higher mean ADC values than lesions with HER2-neu-negative cases, the differences were not statistically significant [24, 25]. ADC values in HER2-positive breast cancer were found to be significantly higher than in HER2-negative breast cancer, according to multiple studies [26–28].

These findings, however, were at odds with those of Mao et al., who demonstrated that there was no statistically significant difference in ADC values between HER2-positive and HER2-negative groups ($p=0.126$) [29]. Furthermore, unlike our current results, Roknsharifi et al. stated that there was no meaningful association between HER2 status and ADC values [30].

HER2-positive BC may be more heterogeneous than HER2-negative breast cancer, which may explain this controversy. Recent research by Kim et al. revealed high intratumoral kinetic heterogeneity in HER2-positive breast cancer [31]. ADC value measurements in breast cancer might be affected by the higher heterogeneity.

The current study's variation can be attributed to the enhanced angiogenesis that inhibits diffusion restriction [32].

According to the current results, with a moderate sensitivity of 65.7% and specificity of 60%, the mean ADC value to identify cases with positive HER2 was $>0.885\times10^{-}3$ mm_2/s.

Larger scale studies are still needed to confirm the use of MRI in identifying molecular subtypes of breast cancer. Still, in the meantime, it can be used as a noninvasive method of diagnosis.

Limitations

The number of cases was relatively large; however, more cases are still needed, especially the luminal b cases with HER2-negative receptors, to improve the statistical outcome. The relatively long duration of the scan results in some motion artifacts, especially in older patients.

Conclusions

Magnetic resonance imaging of the breast is a promising noninvasive method for identifying breast cancers with the HER2 molecular subtype. Combining the various radiological features could offer a conclusion with a sufficient degree of identifying the positive HER2 lesions.

Abbreviations

MRI	Magnetic resonance imaging
ER	Estrogen receptor
PR	Progesterone receptor
HER2	Human epidermal growth factor
HR	Hormone receptor
NACT	Neoadjuvant chemotherapy
US	Ultrasound
DWI	Diffusion-weighted imaging
DCE-MRI	Dynamic contrast-enhanced magnetic resonance imaging
EPI	Echo planner imaging
TR	Repetition time
TE	Time to echo
NEX	Number of excitations
ADC	Apparent diffusion coefficient
ROI	Region of interest
GRE	Gradient
T1	Longitudinal relaxation time
T2	Transverse relaxation time
WI	Weighted images
STIR	Short tau inversion recovery
MIP	Maximum intensity projection
FOV	Field of view
SPSS	Statistical package for social science
SD	Standard deviation
ROC	Receiver operating characteristic curve
P	Probability
TN	Triple negative
AUC	Area under curve
PPV	Positive predictive value
NPV	Negative predictive value
CI	Confidence interval
OR	Odd's ratio

Acknowledgements

We are grateful to our patients who accepted to participate in our study.

Author contributions

All authors have read and approved the manuscript. The study concept and design were proposed by DB and HS. Statistical analysis of data was performed by AA and DB. Writing the original manuscript was prepared by AA and AE. Preparing figures and tables was performed by AE, AA, and DB. Revision of the manuscript for important intellectual content was performed by AE, DB, and HS.

Funding

The authors state that this work has not received any funding.

Availability of data and materials

All the scientific data are available and presented in the manuscript. The source data are available from the corresponding author upon reasonable request.

Declarations

Ethics approval and consent to participate

Written informed consent was waived by the Institutional Review Board (IRB), Institutional Review Board (IRB) was obtained, IRB approval: MD.22.01.578.

Consent for publication

All the patients were consented and informed of possible research publication. All authors hereby confirm all the copyrights if such work will be accepted in the Journal of Egyptian Journal of Radiology and Nuclear Medicine (EJRNM).

Competing interests

The authors declare that they have no competing interests.

Received: 20 May 2024 Accepted: 30 September 2024
Published online: 15 October 2024

References

1. Bray F, Ferlay J, Soerjomataram I et al (2020) Erratum: global cancer statistics 2018: GLOBOCAN estimates of incidence and mortality worldwide for 36 cancers in 185 countries. Ca Cancer J Clin 70(4):313

2. Rostom Y, Abdelmoneim S-E, Shaker M et al (2022) Presentation and management of female breast cancer in Egypt. Eastern Mediterr Health J. 28(10):725
3. Walter V, Fischer C, Deutsch TM et al (2020) Estrogen, progesterone, and human epidermal growth factor receptor 2 discordance between primary and metastatic breast cancer. Breast Cancer Res Treat 183:137–144
4. Waks AG, Winer EP (2019) Breast cancer treatment: a review. JAMA 321(3):288–300
5. Trop I, LeBlanc SM, David J et al (2014) Molecular classification of infiltrating breast cancer: toward personalized therapy. Radiographics 34(5):1178–1195
6. Boughey JC, McCall LM, Ballman KV et al (2014) Tumor biology correlates with rates of breast-conserving surgery and pathologic complete response after neoadjuvant chemotherapy for breast cancer: findings from the ACOSOG Z1071 (Alliance) Prospective Multicenter Clinical Trial. Ann Surg 260(4):608–616
7. Fessele KL (2022) Bone health considerations in breast cancer. Semin Oncol Nurs 38(2):151273
8. Portnow LH, Kochkodan-Self JM, Maduram A et al (2023) Multimodality imaging review of HER2-positive breast cancer and response to neoadjuvant chemotherapy. Radiographics 43(2):e220103
9. Park VY (2020) Expanding applications of MRI-based radiomics in HER2-positive breast cancer. EBioMedicine 1:61
10. Association WM (2013) World medical association declaration of Helsinki: ethical principles for medical research involving human subjects. JAMA 310(20):2191–2194
11 Metwally SA, Abo-Shadi MA, Abdel Fattah NF et al (2021) Presence of HPV, EBV and HMTV viruses among Egyptian breast cancer women: Molecular detection and clinical relevance. Infect Drug Resist 14:2327–2339
12. Ng CG, Mohamed S, Kaur K et al (2017) Perceived distress and its association with depression and anxiety in breast cancer patients. PLoS ONE 12(3):e0172975
13. Muller KE, Marotti JD, Tafe LJ (2019) Pathologic features and clinical implications of breast cancer with HER2 intratumoral genetic heterogeneity: an institutional review. Am J Clin Pathol 152(1):7–16
14. Bitencourt AGV, Gibbs P, Saccarelli CR et al (2020) MRI-based machine learning radiomics can predict HER2 expression level and pathologic response after neoadjuvant therapy in HER2 overexpressing breast cancer. EBioMedicine 61:103042
15. Darwish AD, Helal AM, El-Din NHA et al (2017) Breast cancer in women aging 35 years old and younger: the Egyptian National Cancer Institute (NCI) experience. The Breast 31:1–8
16. Algazzar MAA, Elsayed EEM, Alhanafy AM et al (2020) Breast cancer imaging features as a predictor of the hormonal receptor status, HER2neu expression and molecular subtype. Egypt J Radiol Nucle Med 51:1–10
17. Elias SG, Adams A, Wisner DJ et al (2014) Imaging features of HER2 overexpression in breast cancer: a systematic review and meta-analysis. Cancer Epidemiol Biomark Prev 23(8):1464–1483
18. Chen P, Zhao S, Guo W, Shao G (2023) Dynamic contrast-enhanced magnetic resonance imaging features and apparent diffusion coefficient value of HER2-positive/HR-negative breast carcinoma. Quant Imaging Med Surg 13(8):4816
19. Zhang H, Li Y, Moran MS et al (2015) Predictive factors of nipple involvement in breast cancer: a systematic review and meta-analysis. Breast Cancer Res Treat 151:239–249
20. Rouanet P, Roger P, Rousseau E et al (2014) HER 2 overexpression a major risk factor for recurrence in pT1a-bN0M0 breast cancer: results from a F rench regional cohort. Cancer Med 3(1):134–142
21 Joensuu K, Leidenius M, Kero M et al (2013) ER, PR, HER2, Ki-67 and CK5 in early and late relapsing breast cancer—reduced CK5 expression in metastases. Breast Cancer: Basic Clinic Res 7:S10701
22. Payandeh M, Shahriari-Ahmadi A, Sadeghi M et al (2016) Correlations between HER2 expression and other prognostic factors in breast cancer: inverse relations with the Ki-67 index and P53 status. Asian Pac J Cancer Prev 17(3):1015–1018
23. Mohmmed EA, Ramadan SS, El-Saiid AS et al (2021) Frequency and clinical features of over-expressed her2 in Egyptian breast cancer women patients. Egypt J Hospit Med 85(1):3431–3435
24. López-García MÁ, Carretero-Barrio I, Pérez-Míes B et al (2020) Low prevalence of HER2-positive breast carcinomas among screening detected breast cancers. Cancers 12(6):1578
25. Rupa R, Thushara R, Swathigha S et al (2020) Diffusion weighted imaging in breast cancer–Can it be a noninvasive predictor of nuclear grade? Indian J Radiol Imag 30(01):13–19
26 Kim EJ, Kim SH, Park GE et al (2015) Histogram analysis of apparent diffusion coefficient at 3.0 t: correlation with prognostic factors and subtypes of invasive ductal carcinoma. J Magnet Reson Imag. 42(6):1666–1678
27. Horvat JV, Iyer A, Morris EA et al (2019) 2019 Histogram analysis and visual heterogeneity of diffusion-weighted imaging with apparent diffusion coefficient mapping in the prediction of molecular subtypes of invasive breast cancers. Contrast Media Molecul Imag 1:2972189
28. Du S, Gao S, Zhang L et al (2021) Improved discrimination of molecular subtypes in invasive breast cancer: comparison of multiple quantitative parameters from breast MRI. Magn Reson Imag 77:148–158
29. Mao C, Jiang W, Huang J et al (2022) Quantitative parameters of diffusion spectrum imaging: HER2 status prediction in patients with breast cancer. Front Oncol 12:817070
30. Roknsharifi S, Fishman MDC, Agarwal MD et al (2019) The role of diffusion weighted imaging as supplement to dynamic contrast enhanced breast MRI: can it help predict malignancy, histologic grade and recurrence? Acad Radiol 26(7):923–929
31. Kim JJ, Kim JY, Suh HB et al (2022) Characterization of breast cancer subtypes based on quantitative assessment of intratumoral heterogeneity using dynamic contrast-enhanced and diffusion-weighted magnetic resonance imaging. Europ Radiol 32:1–12
32. Martincich L, Deantoni V, Bertotto I et al (2012) Correlations between diffusion-weighted imaging and breast cancer biomarkers. Eur Radiol 22:1519–1528

Publisher's Note